Electronic Supplementary Material (ESI) for Journal of Materials Chemistry A.
This journal is © The Royal Society of Chemistry 2022

Supporting Information

Largely improved generating energy density, efficiency, and fatigue life of DEG by designing TiO_2/LNBR/SiR DE composites with self-assembled structure

Xuesong Hao[⊥,1], Xueying Liu[⊥,1], Yingjie Jiang[1], Chaojun Wang[1], Haibin Sun[1], Wenpeng Zang[1], Nanying Ning*[,1,2,3], Ming Tian*[,1,2,3] and Liqun Zhang[1,2,3]

1. State Key Laboratory of Organic-Inorganic Composites, Beijing University of Chemical Technology, Beijing 100029, China;

2. Beijing Advanced Innovation Center for Soft Matter Science and Engineering, Beijing University of Chemical Technology, Beijing 100029, China;

3. Key Laboratory of Carbon Fiber and Functional Polymers, Ministry of Education, Beijing University of Chemical Technology, Beijing 100029, China;

⊥ Xuesong Hao and Xueying Liu contributed equally to this work and they should be regarded as co-first authors.

* Corresponding authors. Tel.: 86 10 64456158; Fax: 86 10 64433964.

E-mail addresses: tianm@mail.buct.edu.cn (M. Tian);

ningny@mail.buct.edu.cn (N. Ning)

Section S1: Characterization methods

***^{1}H-NMR Spectroscopy*:** The ^{1}H NMR spectra was performed on a 600 MHz instrument of the Bruker AV600 NMR spectrometer produced in Germany, and $CDCl_3$ was used as the solvent.

***Fourier transform infrared spectroscopy (FT-IR)*:** The structural analysis of LNBR was characterized by Fourier transform infrared spectroscopy (Tensor 27, Bruker Optik, Germany) from 4000 to 500 cm^{-1} in transmission mode with a disc of KBr.

***Gel permeation chromatography (GPC)*:** The weight-average molecular weight (M_w) was measured by gel permeation chromatography (GPC) on a Waters Breeze instrument equipped with three Waters columns (Steerage HT3_HT5_HT6E) by using THF as the eluent (1 mL/min) and a Waters 2410 refractive index detector. A polystyrene standard was used for calibration.

***Scanning electron microscope (SEM)*:** The microstructure of dielectric composites and elemental mapping analysis of energy-dispersive spectroscopy (EDS) were investigated by using a scanning electron microscope (SEM, S-4800) at accelerated electron energy of 5.0 kV.

***Atomic force microscope (AFM)*:** A Bruker Multi Mode AFM with a Nanoscope IV controller in Quantative Nanomechanical Mapping (AFM-QNM) mode was used to measure the nanomechanical properties of SiR composites. The yellow region represents SiR matrix with low Young's modulus and the blue region represents TiO_2 particle with high Young's modulus.

***Density functional theory (DFT)*:** The structure and intersegmental interaction of

hydrogen bonding in samples were studied by DFT method at the B3LYP/6-31+G* level by the Gaussian 09 software package. The B3LYP functional combines Becke's three parameter (B3) gradient-corrected exchange functional and the nonlocal correlation functional by Lee, Yang, and Parr (LYP) gradient-corrected correlation functional. Optimizations of all the geometries were carried out in the gas phase, and all the energies were corrected for zero-point vibrational energy.

***Contact angle*:** An optical contact angle meter (Kruss DSA 100, Germany) was used to measure the contact angle of LNBR and SiR, and drop of deionized water and ethylene glycol at ambient temperature. The surface tension of LNBR (γ_{LNBR}) and SiR (γ_{SiR}), and the interfacial tension of LNBR/SiR blend ($\gamma_{LNBR/SiR}$) can be calculated by the Equations below:

$$\left(1+\cos\theta_{H_2O}\right)\gamma_{H_2O}=4\left(\frac{\gamma_{H_2O}^{d}\gamma_s^d}{\gamma_{H_2O}^{d}+\gamma_s^d}+\frac{\gamma_{H_2O}^{p}\gamma_s^p}{\gamma_{H_2O}^{p}+\gamma_s^p}\right) \tag{S1}$$

$$\left(1+\cos\theta_{(CH_2OH)_2}\right)\gamma_{(CH_2OH)_2}=4\left(\frac{\gamma_{(CH_2OH)_2}^{d}\gamma_s^d}{\gamma_{(CH_2OH)_2}^{d}+\gamma_s^d}+\frac{\gamma_{(CH_2OH)_2}^{p}\gamma_s^p}{\gamma_{(CH_2OH)_2}^{p}+\gamma_s^p}\right) \tag{S2}$$

$$\gamma_s=\gamma_s^d+\gamma_s^p \tag{S3}$$

$$\gamma_{LNBR/SiR}=\gamma_{LNBR}+\gamma_{SiR}-2\left(\gamma_{LNBR}^{d}\gamma_{SiR}^{d}\right)^{\frac{1}{2}}-2\left(\gamma_{LNBR}^{p}\gamma_{SiR}^{p}\right)^{\frac{1}{2}} \tag{S4}$$

***Mechanical properties*:** The tensile tests and cyclic stress-strain tests of the samples were performed on dumbbell-shaped samples (length × width × thickness:20 × 4× 0.5 mm^3) using a tensile apparatus (Instron 5567, USA) at room temperature with a tensile rate of 500 mm/min. The elastic modulus of the samples was determined by the slope of the stress-strain curve at 10% strain. For the cyclic stress-strain test, the sample was

stretched to a constant strain of 200% and then carried out loading process without relax time at same speed.

***Crosslinking density*:** The crosslinking density of samples was evaluated by a low field NMR analyzer (Niumag Corporation, China) at 20 MHz proton resonance frequency and a magnetic field strength of 0.5 T. The samples (5 cm long and 0.5×0.5 cm in cross-sectional area, about 1.5 g) were placed in a cylindrical glass tube (10 mm in diameter) and then inserted into the probe of the low field NMR analyzer.

The basic principle of Low field NMR studying the structure and dynamics characterization of elastomers consists he spin-spin relaxation time T_2. The spin-spin relaxation time T_2 depends on the mobility of chemical components of an elastomer. Normally, the stiffness of fractions like polymer chains and polymer-interfaces is described by correlation times of different orders. Thus, the transverse NMR relaxation decay can be separated by functions which can be identically referred to these fractions. The contribution of each fraction to the signal is proportional to its content in a sample. Usually, the nuclei of polymer network protons are quite movable and their T_2 vary within 0.3-15 ms depending on the crosslinking degree. The more heterogeneous structure of an elastomer caused by the network cross-linking, the wider the T_2 slow distribution. Based on the XLD Model, the crosslinking density (V_c) can be calculated by the following Equation:

$$V_C = \frac{\rho}{M_c} = \frac{5\rho N\sqrt{q}}{3C_\infty M_{ru}} \tag{S5}$$

Where, ρ: density of sample; M_c: number average molecular weight of the elastomer (g/mol); N: the number of bonding of the main chain; q: the anisotropic

factor; C_∞: flexibility parameter of the elastomer chain; M_{ru}: molecular weight of monomer unit (g/mol).

***Dielectric properties*:** The dielectric properties of samples were measured by a broadband dielectric spectrometer (BDS, Concept 40, Novocontrol GmbH, Germany) over the frequency range of 10^{-1} Hz to 10^6 Hz at room temperature. The samples have a diameter of 10 mm and a thickness of 0.5 mm.

***Conductivity*:** A high resistance meter (GEST-121, Beijing Guance, China) was used to measure the conductivity of samples, which is the reciprocal of volume resistivity. The conductivity (σ) is calculated by using the following Equation:

$$\sigma = \frac{4L}{R_v \pi d^2} \tag{S6}$$

where L is the thickness of the sample, R_v is the resistance of the sample and d is the diameter of the sample.

***Electrical charge leakage rate*:** The voltage versus time can be recorded by oscilloscope, and corresponding circuit diagram is shown in Fig. S7(a). The steps of experiment are as following: firstly, set up the circuit, apply the specified bias voltage value (U_{input}= 5.0 kV) by turning on the high-voltage DC power and close both switch S_1 and S_2; Secondly, open both switch S_1 and S_2; Finally, only close the switch S_2, and the output voltage value (U_{output}) can be obtained. The electrical charge leakage rate can be calculated through Equation (S7):

$$Electrical\ charge\ leakage\ rate = 1 - \frac{Q_{output}}{Q_{input}} \times 100\% = 1 - \frac{U_{output}}{U_{input}} \times 100\% \tag{S7}$$

where Q_{input} and Q_{output} represent the input electrical charge and output electrical charge, respectively.

***Electric breakdown strength (E_b) and bias breakdown voltage under uniaxial strain (U_{1b})*:** The E_b and U_{1b} was measured by a home-made equipment. Conductive carbon grease was coated onto both sides of the DE film as compliant electrodes. The dimension of working area of DE film was 80×20×0.5 mm^3. A linear motor (E1100, Linmot Co. Ltd.) was used to stretch the DE film (600 mm/min) and record the uniaxial strain. The uniaxial stretching direction was perpendicular to the long side of the work area. The voltage was supplied by a high-voltage direct current generator (DTZH-60, Wuhan Dotek Electric) under a ramp rate of 1 kV/s until electric breakdown.

***Energy harvesting performance*:** The experimental devices and working circuit of the measurement of uniaxial DEG harvesting performance are shown in Fig. S8. Conductive carbon grease was coated onto both sides of the DE film as compliant electrodes. The dimension of working area of DE film is 80×20×0.5 mm^3. The capacitance of sample under different uniaxial strains is measured and recorded by a Digital Multimeter (DMM6500, Tektronix, USA). C_P is parallel transfer capacitor in the circuit as a protective role for avoiding electrical breakdown, which is usually set as 1.3 times of C_1. Both doide and resistance are used to protect circuit. The initial prestrain of as-prepard samples and VHB 4905 is set as 25% and 100%, respectively, because the formers have better elasticity than the latter. The input mechanical energy (W_{mech}) and the change of voltage across DE film are recorded by force sensor and oscilloscope, respectively.

The DEG energy harvesting process or lighting up LEDs process was carried out through the following four steps: (i) stretching process: uniaxial stretching was

performed on the DEG subassembly under a constant speed of 600 mm/min by using a linear motor from released state to stretched state; (ii) boosting process: close all the switches, make the DC source with preset input voltage U_1 charge the DE film and C_P for 5 s, and observe the brightness of the LEDs; (iii) releasing process: open all the switches, and releasing the DEG subassembly under a speed of 600 mm/min to released state; (iv) harvesting process or lighting up LEDs process: close switch S_2 and switch S_3 to make the DEG and C_P discharge the LEDs as well as the oscilloscope record output voltage U_2, and observe the brightness of the LEDs.

Section S2: Figures and Tables

Contents

S2.1 Characterization of LNBR

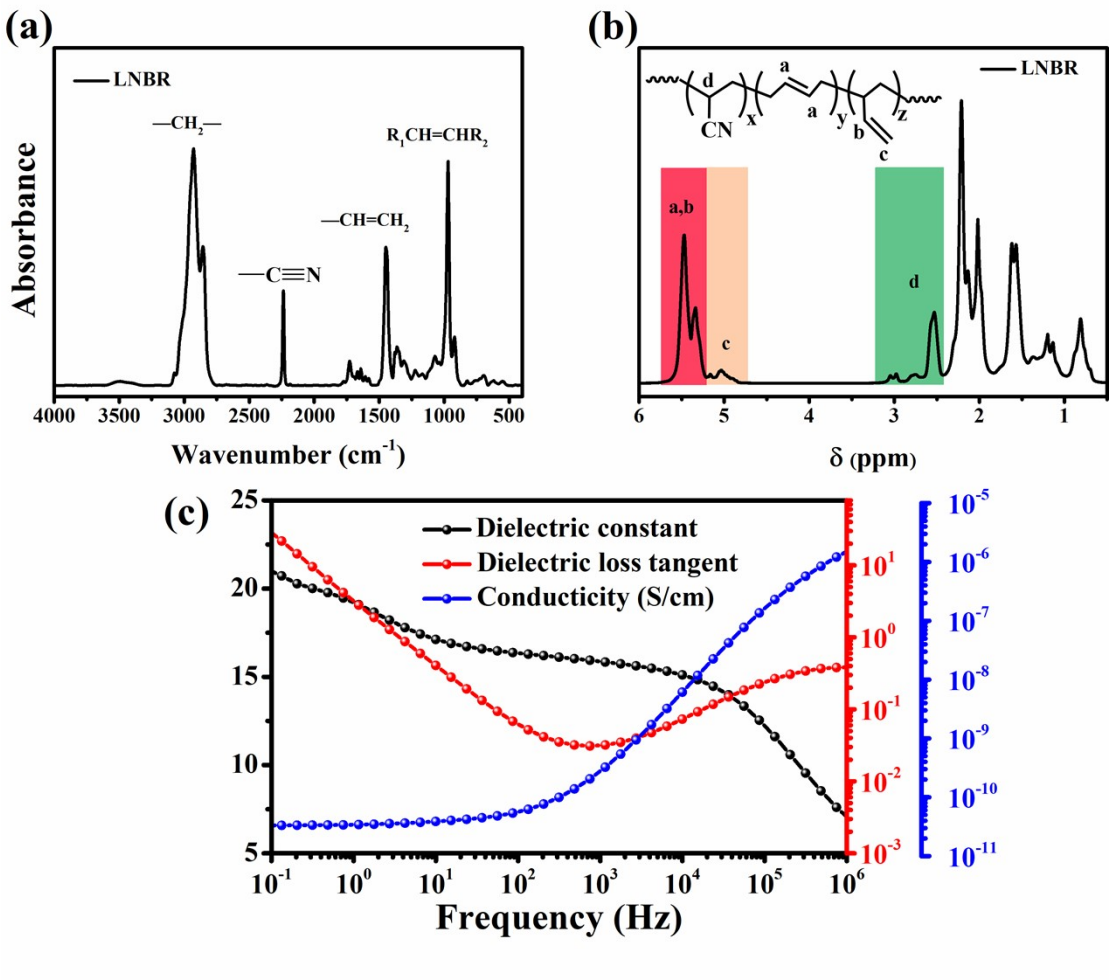

Figure S1. (a) FTIR spectra, (b) ^{1}H NMR spectra and (c) dielectric properties of LNBR.

Liquid acrylonitrile-butadiene rubber (LNBR, M_w=8.8×10^3 g·mol^{-1}) was obtained from Lanzhou Petrochemical Co., Ltd. (China), and its structure is characterized by FTIR spectrum (see Fig. S1(a)). It can be found that the peak at 2928 cm^{-1}, 2237 cm^{-1}, 1463 cm^{-1} and 970 cm^{-1} are assigned to the symmetric stretching of -CH_2-, the stretching vibration of -C≡N, wagging vibration of 1,2-CH=CH_2 and wagging vibration of 1,4-CH=CH-, respectively. In addition, the content of cyano group in such LNBR was also evidenced by ^{1}H NMR spectrum (see Fig. S1(b)). The characteristic bimodal peak at

5.2-5.9 ppm were assigned to the protons of the -C*H*=C*H*- and -C*H*=CH_2. The characteristic peaks at 4.9-5.1 ppm and 2.49-3.2 ppm were assigned to the protons of -CH=CH_2 and the protons adjacent to the cyano group(-C*H*-CN), respectively.

Based on ^{1}H NMR spectra, the content of cyano group in LNBR (*CN(%)*) can be calculated by Equation S8, which is about 44.0%.

$$CN(\%) = \frac{S_d}{\frac{S_{a+b} - 0.5S_c}{2} + \frac{S_c}{2} + S_d} = \frac{4S_d}{2S_{a+b} + S_c + 4S_d} \times 100\% \quad \text{(S8)}$$

Where, S_{a+b}, S_c and S_d are the area of chemical shift of -C*H*=C*H*- and -C*H*=CH_2, -CH=CH_2 and -C*H*-CN, respectively.

The dielectric properties of LNBR are shown in Fig. S1(c). It can be found that the dielectric constant (ε_r), dielectric loss tangent (tan δ) and conductivity (σ) of LNBR are 20.7, 21.8 and 3.34×10^{-11} S/cm at 10^{-1} Hz, respectively.

S2.2 Microstructure

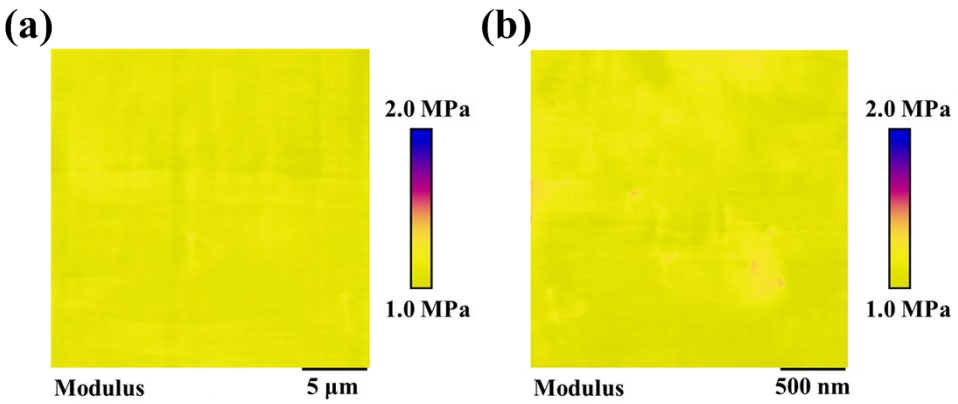

Figure S2. (a) AFM nanomechanical mapping adhesion images of LNBR/SiR blend and (b) its corresponding enlargement.

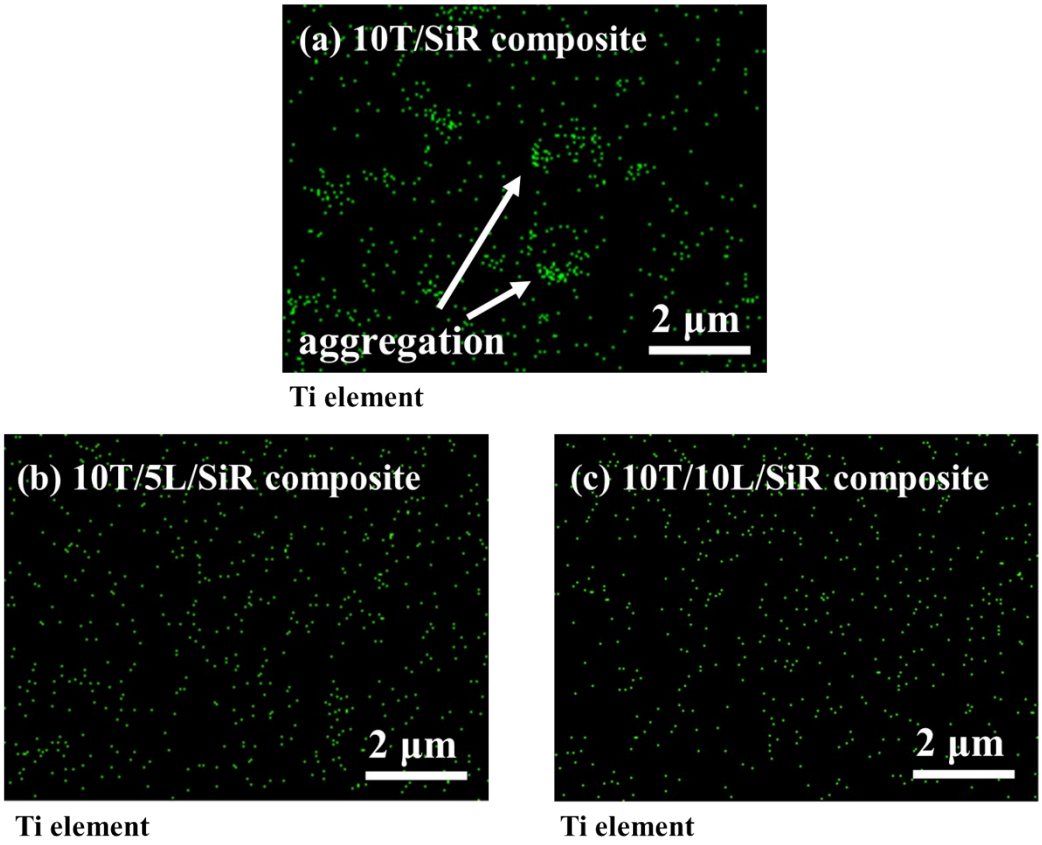

Figure S3. EDS mapping images of Ti element of (a) 10T/SiR composite, (b) 10T/5L/SiR composite and (c) 10T/10L/SiR composite.

The elemental mapping analysis of energy-dispersive spectroscopy (EDS) was employed to directly evidence the dispersed state of TiO_2 particles, as shown in Fig. S3. Significant aggregation of TiO_2 can be observed in TiO_2/SiR composite, whereas the uniform dispersion of TiO_2 particle was observed in TiO_2/LNBR/SiR composites. This is attributed to the largely improved interfacial interaction between LNBR@TiO_2 and SiR matrix in TiO_2/LNBR/SiR composites (see AFM results in Fig. 2).

S2.3 DFT simulation

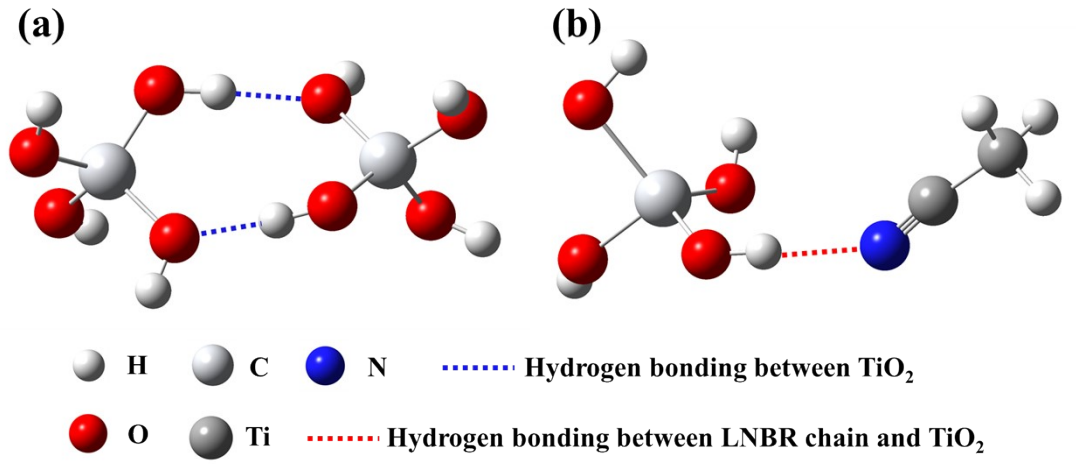

Figure S4. Simulated model of hydrogen bonding: (a) TiO_2/TiO_2 and (b) $LNBR/TiO_2$.

S2.4 Crosslinking density

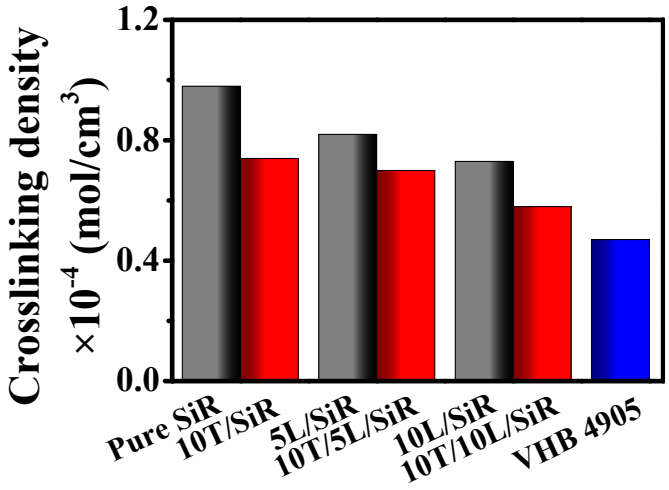

Figure S5. Crosslinking density of all the samples.

S2.5 Dielectric properties

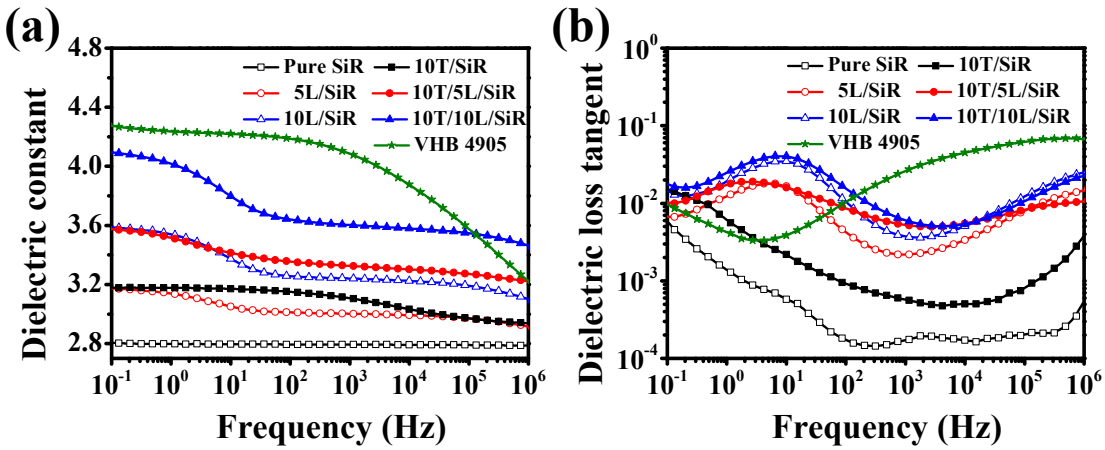

Figure S6. (a) Dielectric constant and (b) dielectric loss tangent versus frequency of pure SiR, LNBR/SiR blends, TiO_2/SiR composite, TiO_2/LNBR/SiR composites and VHB 4905.

S2.6 Energy harvesting performance

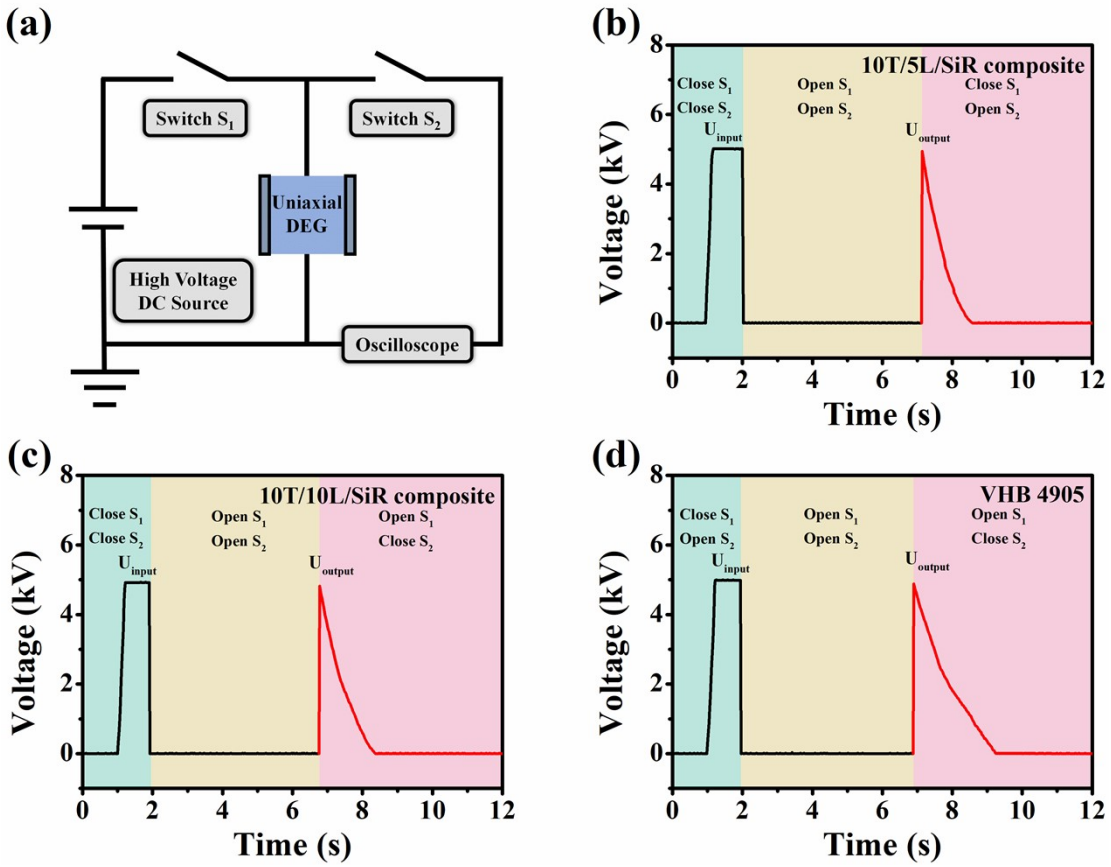

Figure S7. (a) The circuit diagram employed for testing electrical charge leakage rate of DEG; voltage versus time recorded by oscilloscope of (b) 10T/5L/SiR composite, (c) 10T/10L/SiR composite and (d) VHB 4905 under different state of switch.

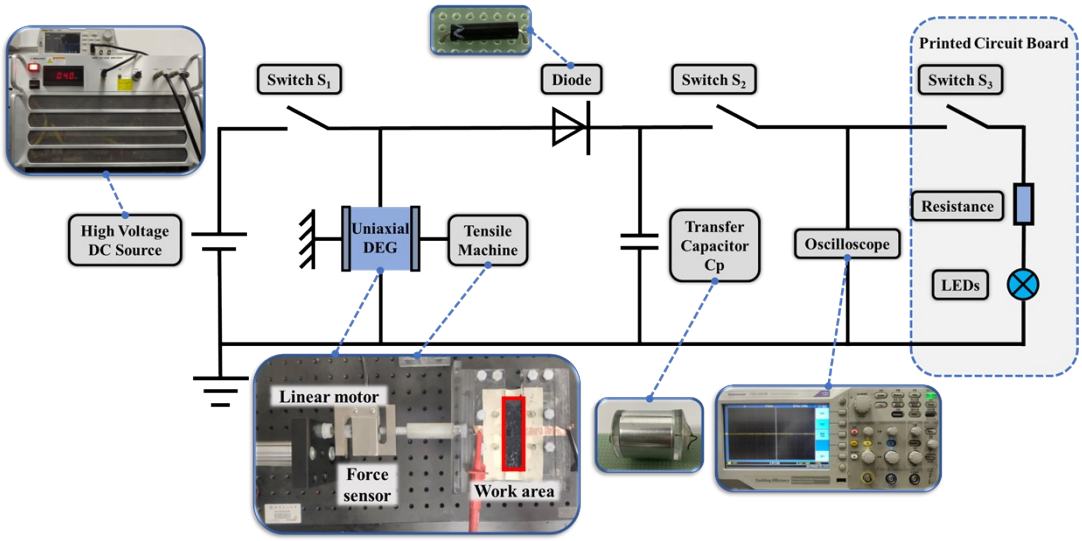

Figure S8. The experimental devices and working circuit of the measurement of uniaxial DEG harvesting performance.

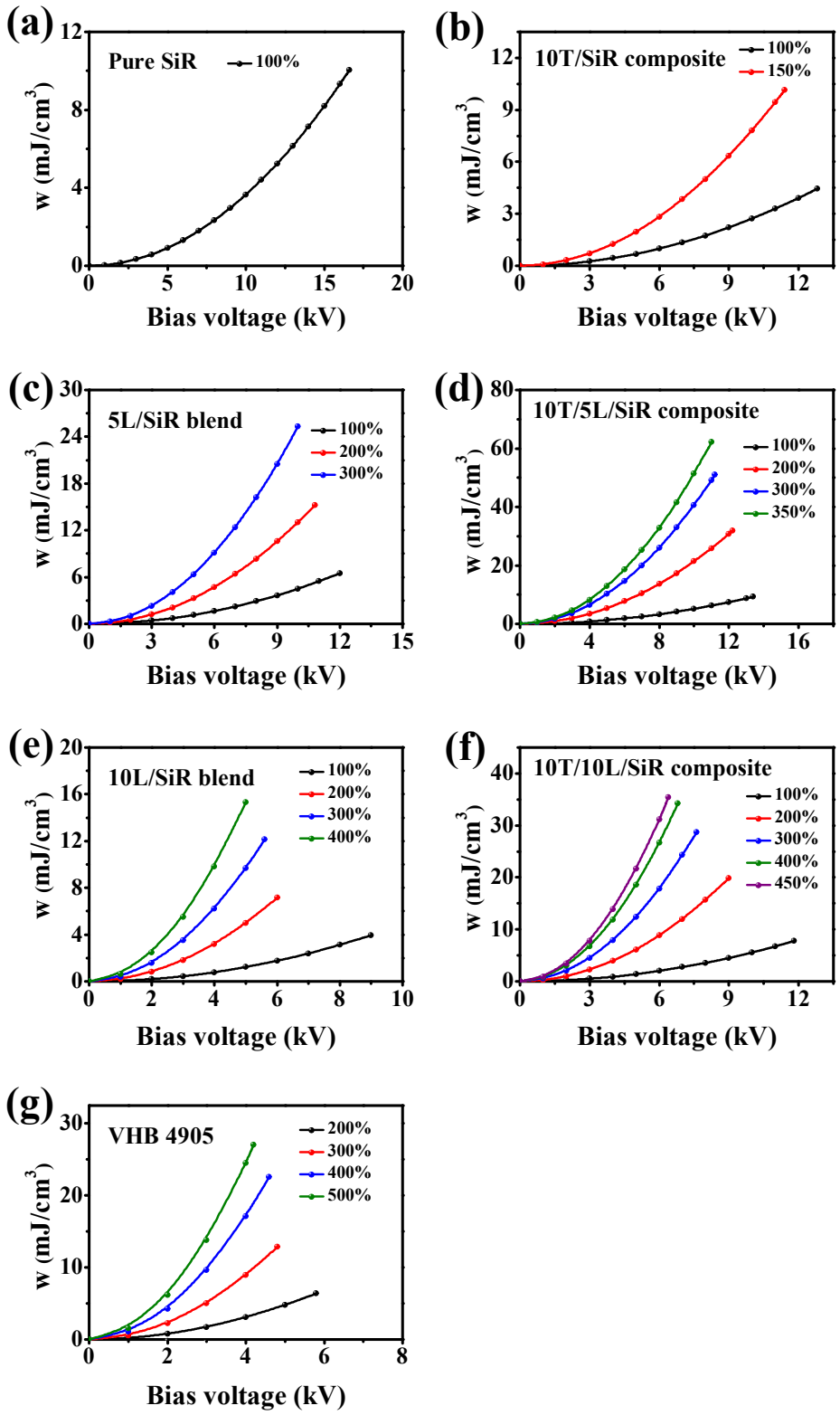

Figure S9. (a)-(g) energy density (w) versus bias voltage under different uniaxial strain and of pure SiR, LNBR/SiR blends, TiO_2/SiR composite, TiO_2/LNBR/SiR composites and VHB 4905.

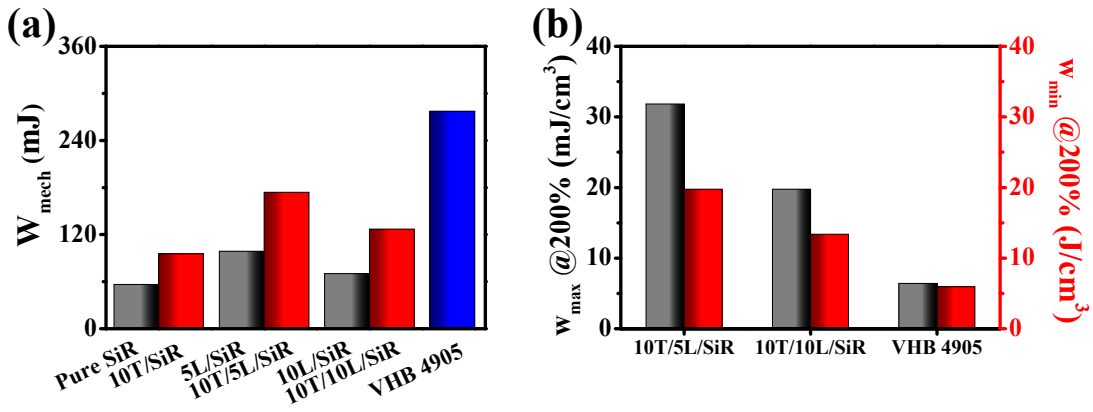

Figure S10. (a) Input mechanical energy (W_{mech}) of all the samples during their maximum energy harvesting process under the U_{1max}; (b) maximum energy density and minimum energy density under 200% uniaxial strain of TiO_2/LNBR/SiR composites and VHB 4905.

S2.7 Compatibility between LNBR and SiR

Table S1 The contact angle and surface tension of SiR and LNBR.

Samples	Contact angle		γ^d (mN/m)	γ^p (mN/m)	γ (mN/m)
	Deionized water	Ethylene glycol			
SiR	114.1°	99.8°	5.70	7.13	12.83
LNBR	95.4°	80.5°	7.56	13.77	21.33

To demonstrate LNBR/SiR blend is a homogeneous structure, the contact angle and surface tension were tested to investigate the compatibility between LNBR and SiR, and the results are shown in Table S1. According to the Equations (S1) to (S4) in Supporting Information, the surface tension of LNBR (γ_{LNBR}) is 12.83 mN/m, surface

tension of γ_{SiR} is 21.33 mN/m and the interfacial tension of LNBR/SiR blend (γ_{Blend}) is 1.21 mN/m. The γ_{Blend} is much smaller than the difference between γ_{SiR} and γ_{LNBR} (8.50 mN/m), indicating a good compatibility between LNBR and SiR.

S2.8 Performance summary

Table S2 Mechanical properties, dielectric properties and density of pure SiR, LNBR/SiR blends, TiO_2/SiR composite, TiO_2/LNBR/SiR composites, VHB 4905 and LNBR.

Sample	Elastic modulus (MPa)	Tensile strength (MPa)	Elongation at break (%)	ε_r @ 10^{-1} Hz	tan δ @ 10^{-1} Hz	Volume Conductivity (S/cm)	Density (g/cm^3)
Pure SiR	0.38	0.37 ±0.02	361 ±30	2.80	0.004	1.34×10^{-15}	0.97
5L/SiR	0.31	0.49 ±0.05	667 ±41	3.17	0.006	2.63×10^{-15}	0.98
10L/SiR	0.25	0.35 ±0.08	1018 ±54	3.58	0.012	4.80×10^{-15}	0.99
10T/SiR	0.44	0.45 ±0.07	448 ±26	3.17	0.014	3.19×10^{-15}	1.05
10T/5L/SiR	0.39	0.84 ±0.05	849 ±34	3.57	0.009	1.56×10^{-15}	1.04
10T/10L/SiR	0.31	0.60 ±0.07	1189 ±67	4.09	0.016	3.40×10^{-15}	1.03
VHB 4905	0.21	0.88 ±0.09	1268 ±32	4.26	0.008	1.90×10^{-15}	0.96
LNBR	-	-	-	20.7	21.8	3.34×10^{-11}	-